# Magnetic response of brickwork artificial spin ice

Jungsik Park, Brian L. Le, Joseph Sklenar, Gia-Wei Chern, Justin D. Watts, and Peter Schiffer

Phys. Rev. B **96**, 024436 — Published 24 July 2017

DOI: 10.1103/PhysRevB.96.024436

# Magnetic response of brickwork artificial spin ice

Jungsik Park[1], Brian L. Le[1], Joseph Sklenar[1], Gia-Wei Chern[2], Justin D., Watts[3], Peter Schiffer[1]

[1]Department of Physics, Frederick Seitz Materials Research Laboratory, University of Illinois at Urbana-Champaign, Urbana, Illinois 61801, USA

[2]Department of Physics, University of Virginia, Charlottesville, Virginia 22904, USA

[3]Department of Chemical Engineering and Materials Science and School of Physics and Astronomy, University of Minnesota, Minneapolis, Minnesota 55455, USA

We have investigated the response of brickwork artificial spin ice to an applied in-plane magnetic field through magnetic force microscopy, magnetotransport measurements, and micromagnetic simulations. We find that, by sweeping an in-plane applied field from saturation to zero in a narrow range of angles near one of the principal axes of the lattice, the moments of the system fall into an antiferromagnetic ground state in both connected and disconnected structures. Magnetotransport measurements of the connected lattice exhibit unique signatures of this ground state. Also, modeling of the magnetotransport demonstrates that the signal arises at vertex regions in the structure – confirming behavior that was previously seen in transport studies of kagome artificial spin ice.

## Introduction

Artificial spin ice systems are two-dimensional arrays of elongated ferromagnetic elements that enable the detailed study of collective magnetic behavior in a system of interacting moments [1,2,3]. The shape anisotropy and the sub-micron length scale result in each ferromagnetic element comprising a single magnetic domain and thus behaving like a giant uniaxial spin in zero applied field. These systems can be constructed either from connected ferromagnetic nanowires or isolated ferromagnetic islands, and in both cases, a range of exotic behavior can be observed that includes new types of frustration, ordering of effective magnetic charges, and a variety of collective dynamics.

A consistent theme in experimental studies of artificial spin ice systems has been the pursuit of collective magnetic ground states in different array geometries. The ground state configuration of the interacting moments is interesting in itself and a good starting point for studying interesting spin dynamics triggered by excitations. Initial efforts attempting to reach the ground state centered around ac demagnetization in which the artificial spin ice is rotated about an axis perpendicular to the sample plane in an oscillating in-plane magnetic field that decreases in magnitude [4]. This method has been applied to various lattices [5,6,7,8,9] and, although it was effective in reducing the collective magnetostatic energy, a global ground state was difficult to achieve (although recently demonstrated with extremely slow field ramping [10]). In recent years, true thermalization of the island systems has been achieved by either making the island moments sufficiently small so that they are subject to thermal fluctuations near or below room temperature, or heating the arrays to near the Curie temperature of the constituent ferromagnetic material. Through both of these methods, perfect ground state ordering was achieved in the square ice system [11,12,13,14], and a variety of thermally induced phenomena above the ground state were seen in square ice and other lattices [12,13,14,15,16,17,18].

We have performed a study of the field response of brickwork artificial spin ice, which shares the same topology as kagome artificial spin ice but with 90° angles between the moments [9,19]. We found that the ground state of this system can be achieved by a single field sweep when the angle of the magnetic field was precisely oriented, in both connected and disconnected artificial spin ice systems. The ground state formation of the connected brickwork artificial spin ice manifests itself in its unique magnetoresistance properties, which can be accurately reproduced with micromagnetic simulations. In addition, the transport behavior appears to be strongly affected by contributions from the vertex regions of the structure despite their relatively small extent, further confirming behavior that was recently demonstrated for the kagome system [20].

**Experimental details and modelling of magnetoresistance**

The geometry of brickwork artificial spin ice is shown in Fig. 1 for both connected nanowire samples and isolated islands. Note that it is closely related to the square ice structure [5], and, like the tetris and shakti lattices [15,16], it is obtained by removing a sublattice of the square ice lattice elements. As illustrated in Fig. 1c, the connected brickwork geometry consists of legs that are connected by vertex regions, and domain walls rest at those vertices in equilibrium in low magnetic fields. Typical examples of our brickwork artificial spin ice samples are shown in scanning electron microscope images in Fig. 2. The samples were prepared with electron beam lithography using a PMGI/PMMA bi-layer resist and a silicon nitride coated silicon wafer. After electron beam exposure and development, 40 nm of permalloy ($Ni_{81}Fe_{19}$) and 2 nm of aluminum were deposited via electron beam evaporation at a base pressure of $10^{-10}$ Torr and a growth rate of 0.5 Å/s, before liftoff. In the resulting structures of brickwork artificial spin ice, the legs of connected arrays and nanoislands for disconnected arrays are roughly 140 nm wide and 660 nm long. The single-domain nature of each leg and nanoisland is corroborated by

magnetic force microscope (MFM) images of the samples as shown in Fig. 3, in which the white and black dots appear at the vertices for the connected pattern, indicating domain walls, and at the ends of the nanoislands, indicating complete island polarization. In these images, as in all of our zero field MFM images, we find that the system follows the same pseudo ice rule as in kagome spin ice where two moments point into each vertex and one points out, or vice versa [21,22]. This was also seen in our previous study of brickwork artificial spin ice after rotational demagnetization [9]. MFM measurements of the effects of field sweeps were taken by mounting the samples on a rotational stage with precision of ±0.04° between the pole pieces of an electromagnet, sweeping the field from saturation to zero and then measuring at ambient temperature.

For magnetotransport measurements, we used an 8-terminal Hall bar geometry, where an excitation current can be injected in a longitudinal direction as schematically shown in Fig. 2c. We measured both the longitudinal resistance, defined as $\frac{V_L(+)-V_L(-)}{I_{ex}}$, and the transverse resistance, defined as $\frac{V_T(+)-V_T(-)}{I_{ex}}$, where $V_L$ and $V_T$ are the measured longitudinal and transverse voltages, and $I_{ex}$ is the excitation current. We show data taken at 17 Hz with an excitation current of 66.7 μA, and we obtained qualitatively consistent data using different frequencies (170 Hz, 1700 Hz) as well as different excitation currents (22.2 μA, 44.5 μA). The data were taken in a Quantum Design PPMS cryostat at room temperature (300 K), and the sample was mounted with the horizontal rotator option of the PPMS so that the in-plane magnetic field could be rotated to any angle with respect to the current. To calibrate the angle between the magnetic field and the excitation current, which is denoted by θ in Fig. 2b, we measured the angular dependence of the longitudinal resistance at 10,000 Oe. In this high-field limit, the longitudinal signal shows a $\cos^2\theta$ symmetry with a maximum at θ = 0° and a minimum at θ = 90°, as expected for anisotropic magnetoresistance [23]. Therefore, within the PPMS, we were able to calibrate the angular position with a precision of 0.25°. When making

magnetoresistance measurements, the field applied was swept at a fixed angle from 10,000 Oe to -10,000 Oe and back to the original field.

To model the magnetoresistance, we carried out finite element micromagnetic simulations at 0 K using the GPU-accelerated micromagnetic simulation package Mumax3 [24], basing the calculation on a segment of the brickwork lattice, which is shown in Fig. 4. We first computed magnetization maps at different fields, using a cell size of 10 × 10 × 40 nm, exchange stiffness constant of $13 \times 10^{-12}$ J/m, and a saturation magnetization value of 640 kA/m that corresponded to a VSM measurement performed for a witness uniform thin film of permalloy. We then created a current density map using the Ansys Maxwell package (version 16.0) [25], which solves the continuity equation in the finite element scheme assuming constant resistivity throughout the structure. This additional step beyond our previous work in the kagome system was necessary to obtain the more accurate current density distribution in the structure. The voltages responsible for transverse and longitudinal magnetoresistance were calculated under an assumption that the magnetoresistance effects observed originated from the anisotropic magnetoresistance (AMR); this phenomenon is associated with the relative angle of the current and the magnetization. We calculated the voltage difference across the sample by taking the line integral of the electric field vector resulting in AMR, $\mathrm{E} = \rho_0 \mathrm{J} + \Delta\rho(\hat{\mathrm{m}} \cdot \mathrm{J})\hat{\mathrm{m}}$, where J is the electric current density vector, $\hat{\mathrm{m}}$ a unit vector in the direction of the local magnetization, $\rho_0$ the isotropic bulk resistivity, and $\Delta\rho$ the anisotropic magnetoresistivity [23], and then used the voltage to calculate the transverse and longitudinal resistance as above. The line integral was performed using the magnetization map from Mumax3 and the paths of line integrals for longitudinal and transverse magnetoresistance are illustrated in Fig. 4. For the transverse resistance simulation, we have chosen a straight line path from point 3 to 4 in Fig. 4 for the simplicity of calculation. We have checked that the inclusion of the short horizontal segments in the path barely changes the result, as illustrated by Fig. 5.

**Data and Analysis**

The ground state of the brickwork lattice is shown in Fig. 1. In this state, the moments along the short sides of the rectangles are aligned in one direction (red arrows). The moments along the long sides of the rectangles are arranged antiferromagnetically, alternating in direction (purple and green arrows). By observing the MFM results we find we can experimentally obtain the ground state of the moments by aligning the applied field near $\theta = 0°$ and sweeping from saturation to zero. Ground state MFM images are shown in Fig. 3, and we can see that the moments are in the configuration described schematically in Fig. 1. Importantly, both the samples composed of isolated islands and those composed of connected nanowires, as well as our micromagnetic simulations displayed the same behavior, demonstrating that the results are robust. The range of field angles that yield the ground state is surprisingly narrow, corresponding to $|\theta| < 0.50 \pm 0.04°$ and $|\theta| < 0.46 \pm 0.04°$ for the MFM measurements of a connected and a disconnected structure respectively. The uncertainty is obtained by analyzing MFM results at multiple angles to bracket the range of the ground state. From micromagnetic simulations, the required angular windows for ground state formation of the connected and disconnected structures are $|\theta| < 1.05 \pm 0.05°$ and $|\theta| < 0.75 \pm 0.05°$ respectively. For angles just outside the range of the ground state, we find that the moments of the long sides of the rectangles are polarized, and the lattice as a whole is thus in a polarized state.

While surprising that the ground state is easily obtained in this system, it can be understood as a consequence of high symmetry of the lattice around $\theta = 0°$, and a lack of symmetry around $\theta = 90°$. At a given three-island vertex, each moment aligned with $\theta = 90°$ has only a single perpendicular nearest-neighbor moment. For the field at $\theta = 0°$, the interactions with that

perpendicular neighbor dominates the magnetostatic energy at low field for the θ = 90° moments, and allow for only a single lowest energy state for a vertex, given the moment aligned with θ = 0° has a fixed direction. As a result, the moments aligned with θ = 90° form an antiferromagnetic ordering. Even a slight tilt of the field at saturation causes the magnetization of the moments aligned with θ = 90° to rotate in one particular direction as the field is reduced, while a θ = 0° field allows the local dipolar energies to dominate in determining the directions of those moments, resulting in the ground state. Indeed, MFM images taken at H = 0 after a field sweep with θ = 2° [as shown in Fig. 6(a-b)] demonstrate the polarization of the moments aligned with θ = 90°, and the moments are collectively in a polarized state rather than the ground state. Note that these MFM images still show the system following the pseudo ice rule, but the local vertices are not in their ground state since the θ = 90° moments are all aligned rather than in opposite directions at each vertex.

The fact that the angular window required for achieving a ground state of the systems is so narrow can be understood from micromagnetic simulations as well by comparing the energy of a polarized state and the ground state configuration in an applied field (recognizing that the field itself polarizes the structure in the field direction). We simulated both magnetization configurations at various fields by setting the initial state of the system as either a ground state or a polarized state and then simulating relaxation in specific applied fields at θ = 0° and at θ = 2°. We then calculated the total energy of the system after the relaxation in each of the four cases at different magnitude fields. Fig. 7 shows the energy difference we obtain from the simulations for both disconnected and connected systems. We found that at most field values for θ = 0°, the ground state energy was lower in energy. By contrast, the polarized state had lower energy for the applied field angle of 2°. We also note that the curves for each angle suddenly converge towards a flat line at around 2000 Oe. At this high field, the initial state of the simulation does not matter and we get essentially the same resulting states.

Fig. 8a and Fig. 9a show our experimental magnetotransport data for field sweeps between -2500 Oe and 2500 Oe at selected angles. In every magnetoresistance plot shown in Fig. 8a and Fig. 9a, the parabolic background and the field reversal symmetry confirm that AMR dominates the electrical transport as expected. The data show sharp features that stem from collective magnetization reversal of individual legs, as has been seen in previous magnetotransport studies of artificial spin ice [20,22,26,27]. For example, for $\theta = 1.5°$ and $\theta = 91.5°$ data, the feature at around -400 Oe corresponds to a collective magnetization reversal of legs that are parallel to the field. The similar discontinuity around -1300 Oe corresponds to a similar event for legs that are perpendicular to the field. The magnitudes of the field at which these reversal events occur and the AMR background of the experimental magnetoresistance are well captured by our modelling results, which are shown in Fig. 8b and Fig. 9b. The agreement with simulation is consistent with the observed agreement in the kagome system [20]. Although the agreement between the simulation and the experiment is good, at $\theta = 1.5°$ for the longitudinal case and $\theta = 91.5°$ for the transverse case the model is less satisfactory. We attribute the simulated discrepancies to the relatively small size of the simulated lattice that cannot fully capture the collective magnetization dynamics of the connected brickwork artificial spin ice, and possibly to the simulations being conducted at zero temperature rather than the finite temperature of the experiments.

The agreement between simulation and experiment allows us to use the simulations to examine the origins of features in the magnetotransport. For example, we previously reported that much of the transverse magnetoresistance signal of connected kagome artificial spin ice arises from the vertices [20]. Based on those findings, we investigated the effect of vertex regions on the transverse magnetoresistance in our brickwork samples. Fig. 10 demonstrates the separate contributions from vertices and legs to the total transverse signal, obtained by separating the portions of the line integrals of the electric field by region of the sample, i.e.,

integrating only over the legs or only over the vertex portions of the path. Consistent with the kagome artificial spin ice, the vertex regions have considerable impact despite the fact that they occupy significantly less area than the legs. This can be easily understood from the symmetry of the system in the sense that the contributions of the legs cancel, while those of the vertices do not [20]. Unlike the kagome case, however, where vertex effects considerably diminish at angles other than 0° and 90°, the vertex regions significantly impact the magnetotransport data in the brickwork lattice at every angle we studied. This is because in kagome lattice, the cancellation effect of legs is not valid at angles other than 0° and 90°.

We find that the magnetotransport properties of the brickwork lattice are very sensitive to the field direction near θ = 0°, as seen in Fig. 11 and 12, where we show magnetoresistance measurements for θ = ± 0.5° and θ = ± 1.5° – noting that a field sweep at θ = 0.5° results in the ground state while θ = 1.5°, does not. Comparing the down sweep curve of the longitudinal data at θ = 1.5° with the one at θ = 0.5° (two plots at the top of Fig. 11a), only one kink exists at around -1300 Oe in the latter. We also observe a significant change of the features between θ = ± 1.5° and θ = ± 0.5° in the transverse data (Fig. 12a). For example, a sudden decrease of the signal shown at θ = 1.5° (black curve) of Fig. 12a at around -400 Oe is not observed at θ = 0.5° (green curve). The sudden decrease in resistance can be understood from the behavior of the moments, since for θ = 1.5°, the legs aligned with θ = 0° experience magnetization reversal around -400 Oe. However, at θ = 0.5°, because the moments enter the ground state configuration in zero field, the magnetization reversal of those legs requires a stronger applied field because their reversal without the ensuing reversal of neighboring perpendicular legs would form a highly unfavorable three-in/three-out vertex state.

**Conclusion**

Our observation of the ground state for both disconnected and connected brickwork artificial spin ice systems marks a surprisingly easy path toward approaching the ground state of such a system without thermalizing. This appears to result from the different symmetries around the primary axes of the system, and suggests that similar effects might be seen in other structures that have similar differences in symmetry. Combined with the effects of vertices on the magnetotransport, this high degree of sensitivity to field angle could potentially serve a purpose in magnetic devices or in the design of novel artificial spin ice structures to access unusual collective behavior.

**Acknowledgments**

This project was funded by the US Department of Energy, Office of Basic Energy Sciences, Materials Sciences and Engineering Division under grant no. DE-SC0010778. This work was carried out in part in the Frederick Seitz Materials Research Laboratory Central Research Facilities, University of Illinois at Urbana-Champaign. Work at the University of Minnesota was supported by the NSF MRSEC under award DMR-1420013, as well as by DMR-1507048.

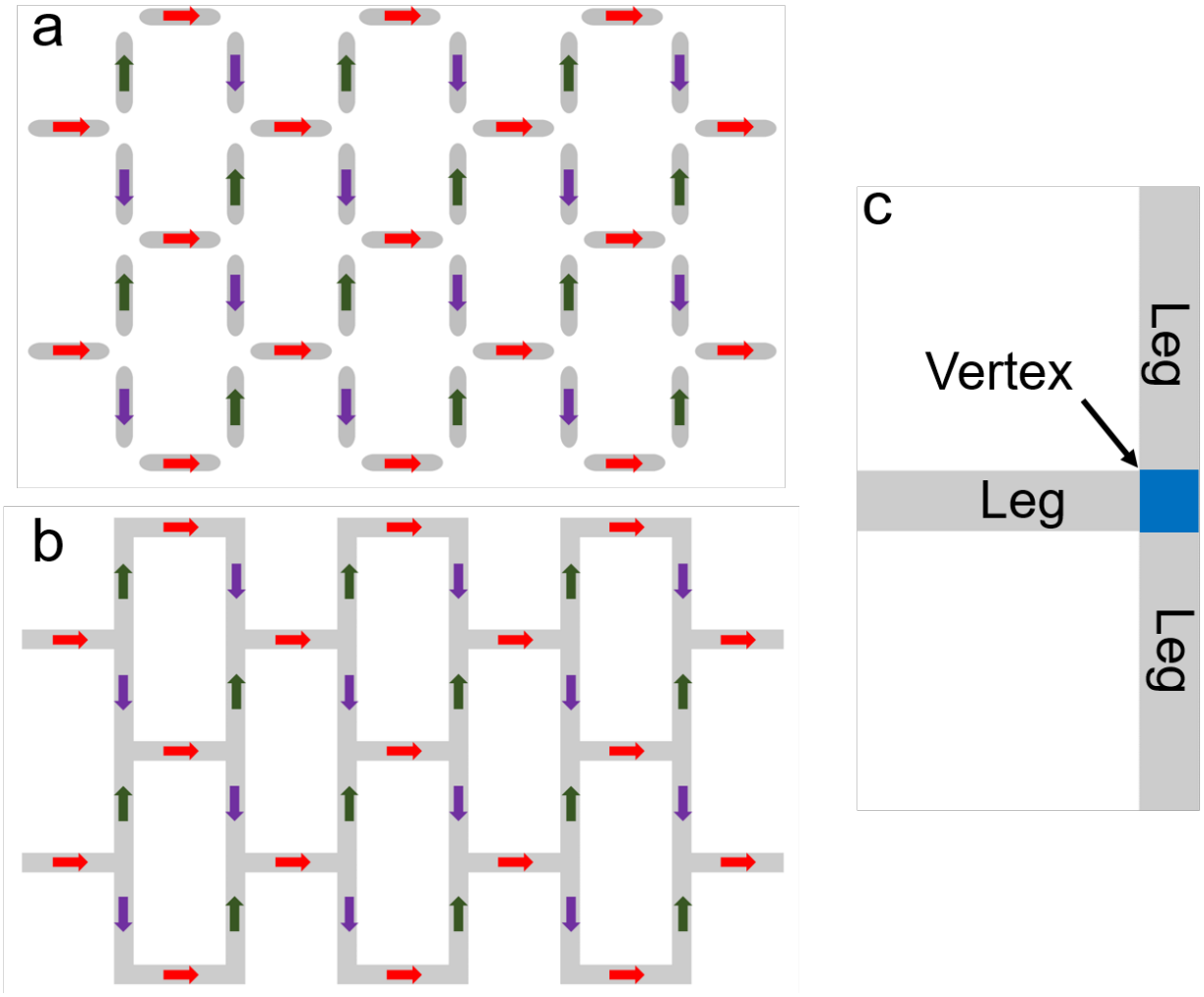


Fig. 1. (a-b) A schematic of (a) disconnected and (b) connected brickwork artificial spin ice. The moment of each island and leg can be treated as a giant uniaxial spin, as indicated by the arrows, where colors correspond to directions. (c) Each junction of the connected lattice can be divided into a “leg” region (grey) and a “vertex” region (blue), the definition of which is used in understanding our magnetotransport simulations.

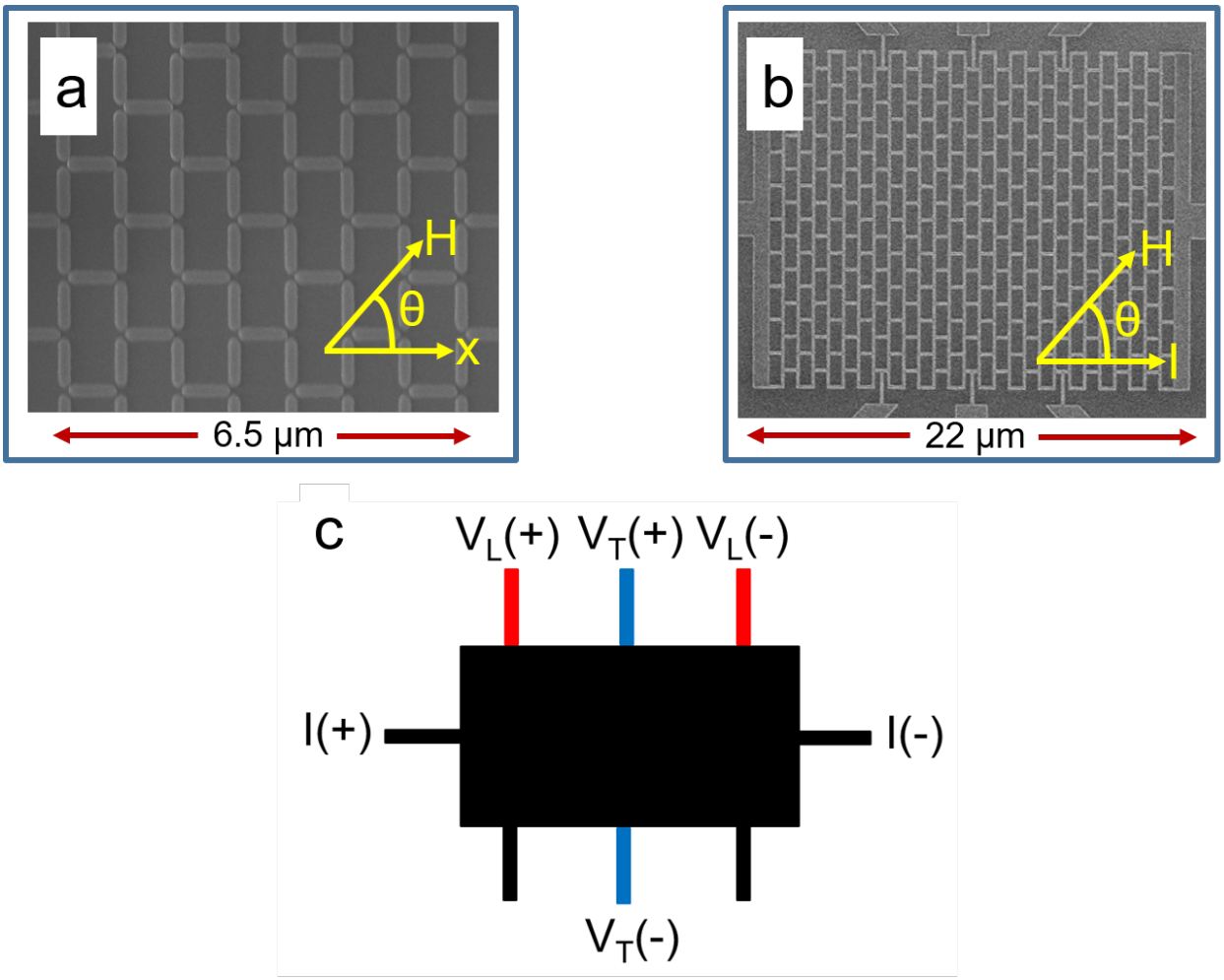


Fig. 2. (a) Scanning electron microscopy (SEM) image of a portion of disconnected brickwork artificial spin ice. The angle between the applied field and the x-axis is defined as θ. (b) SEM image of connected brickwork artificial spin ice. The angle between the applied field and the excitation current direction is defined as θ. (c) A schematic of the leads for magnetotransport measurement.

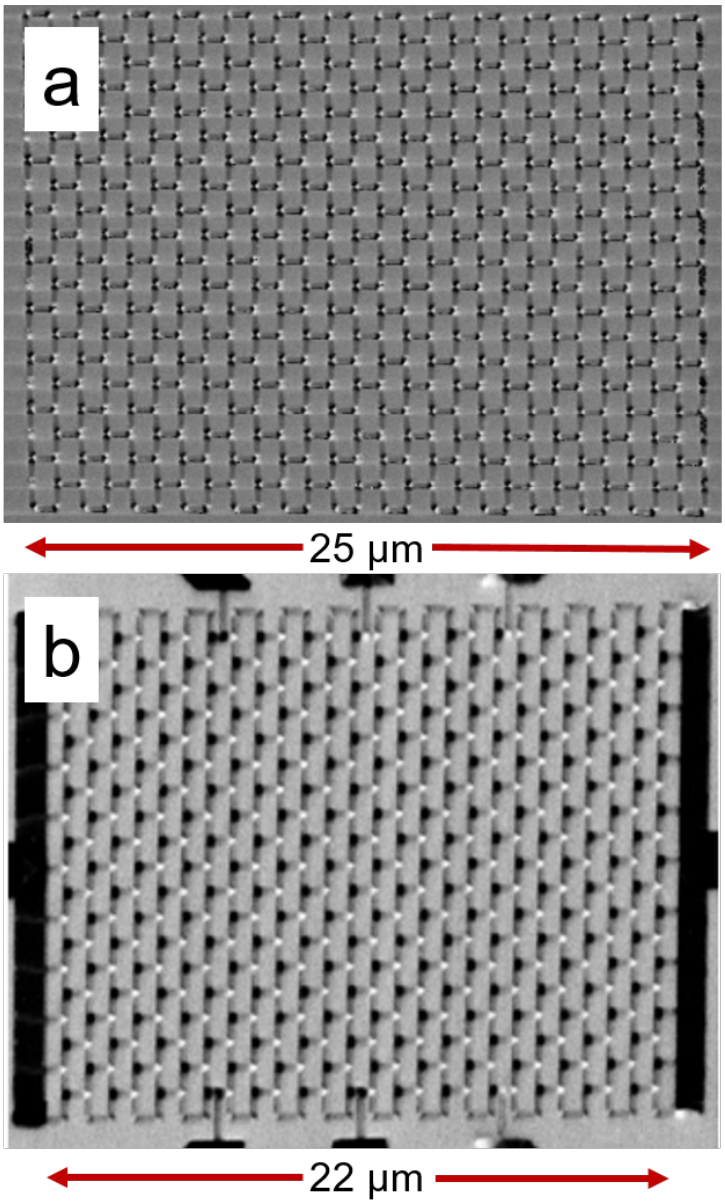


Fig. 3. MFM images of (a) disconnected and (b) connected brickwork artificial spin ice in their ground states in zero magnetic field. For the disconnected islands, a black dot represents a magnetic north pole and white dot represents a magnetic south pole for the islands. In the image for the connected lattice, two-north/one-south vertices appear as black dots, and one-south/two-north vertices appear as white dots.

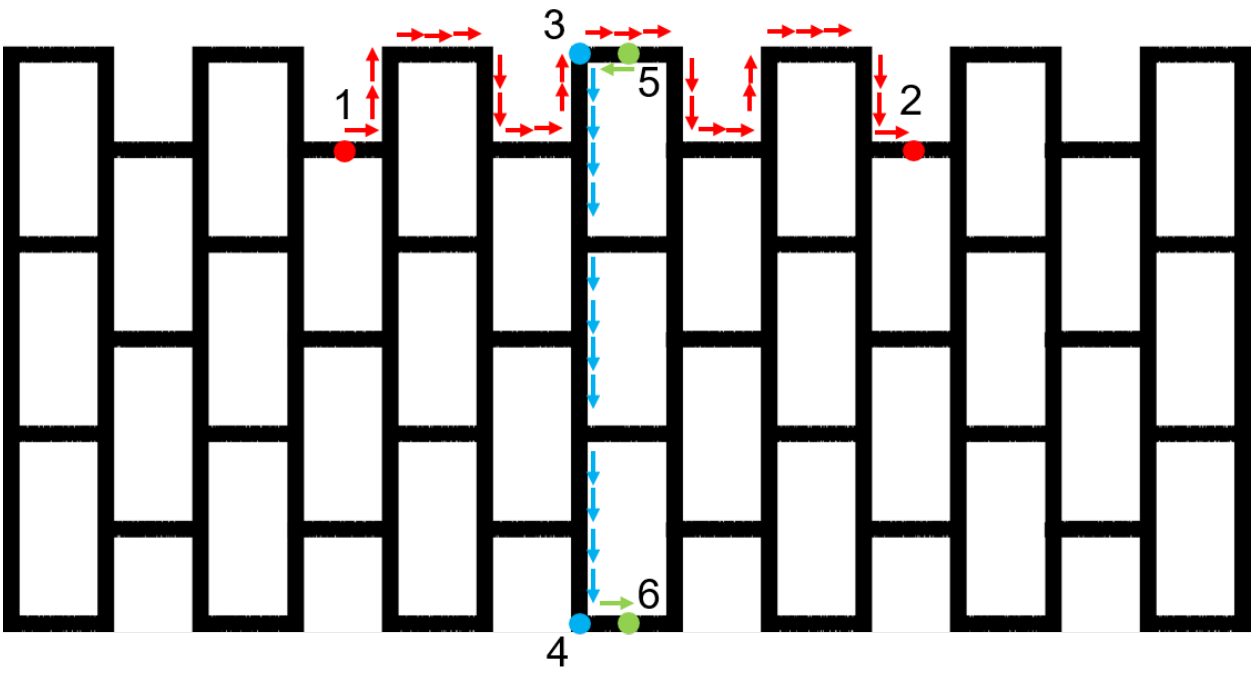


Fig. 4. The geometry of the structure used for micromagnetic simulation. For the simulated longitudinal signal, local electric field vector was integrated along the red path (1 to 2) to obtain the simulated voltage. For the simulated transverse signal, the same calculation was performed along the blue path (3 to 4). The line integral from point 5 to 6, which included the horizontal elements, did not make a qualitatively different result than the one from point 3 to 4.

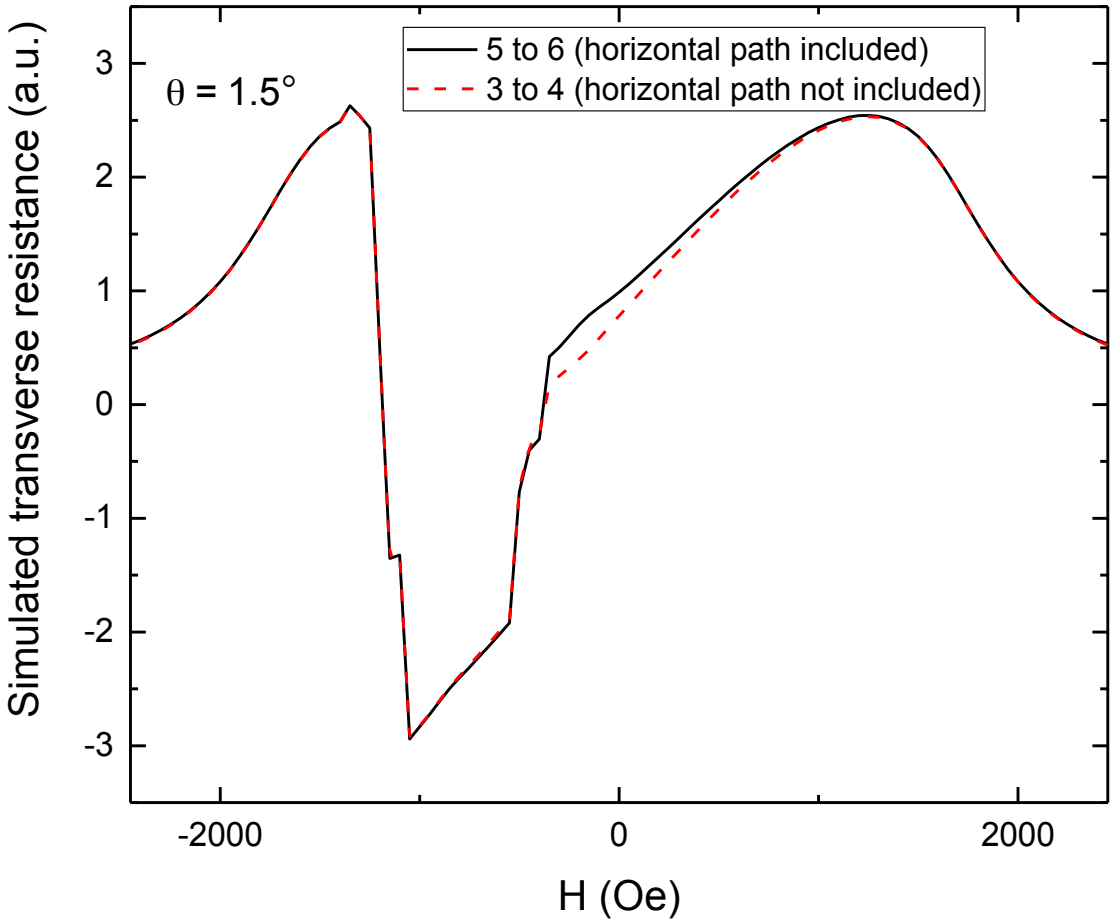


Fig. 5. The comparison of the simulated transverse signal for two different paths. The black curve was obtained by doing the line integral from point 5 to 6 in Fig.4, whereas the red curve was obtained by doing the integral from point 3 to 4.

.

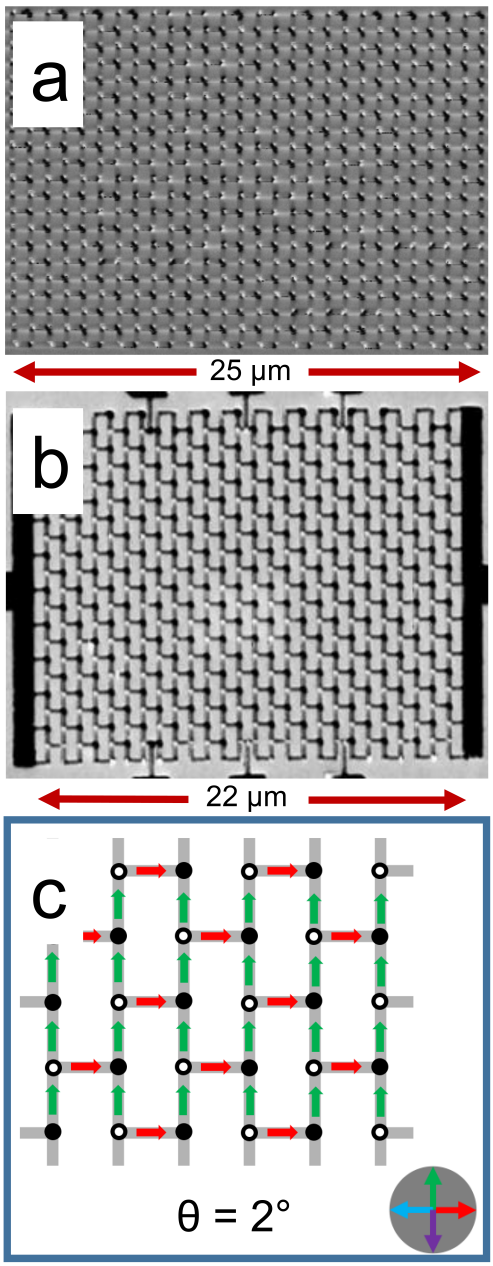


Fig. 6. (a-b) MFM images of (a) disconnected and (b) connected brickwork artificial spin ice after applying the field of 3500 Oe at 2°. The images were taken in zero field. (c) A schematic that shows the magnetization configuration for the MFM image.

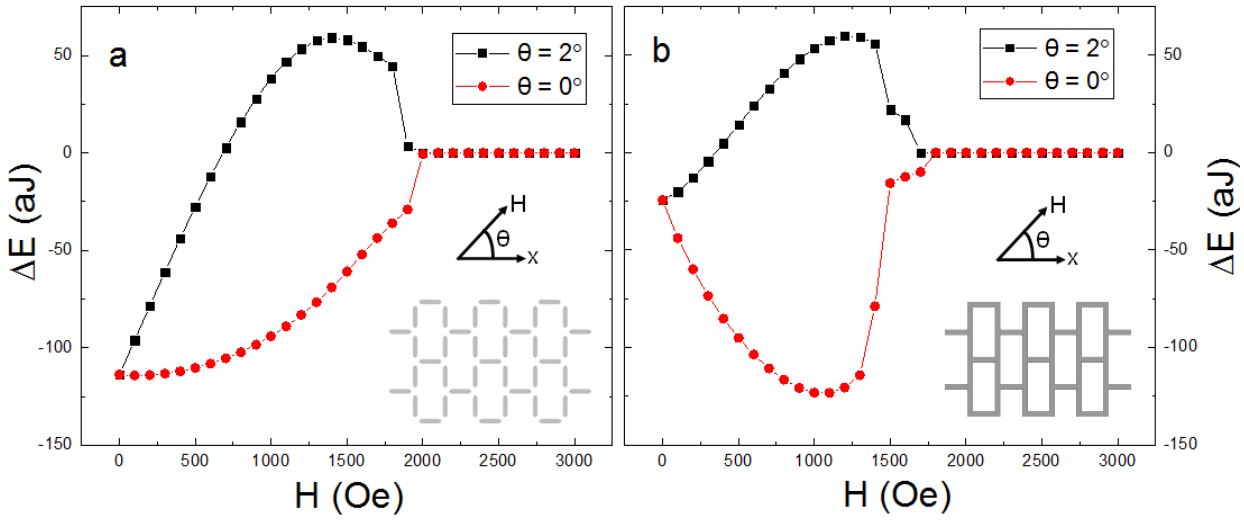


Fig. 7. The field dependence of the simulated energy difference between the states obtained by micromagnetic relaxation from the ground state and from the polarized state. ΔE is defined as the energy obtained after relaxation from the ground state subtracting the energy obtained after relaxation from the polarized state, i.e., $\Delta E = E_{GS} - E_{PS}$. (a) is for the disconnected lattice, and (b) is for the connected lattice.

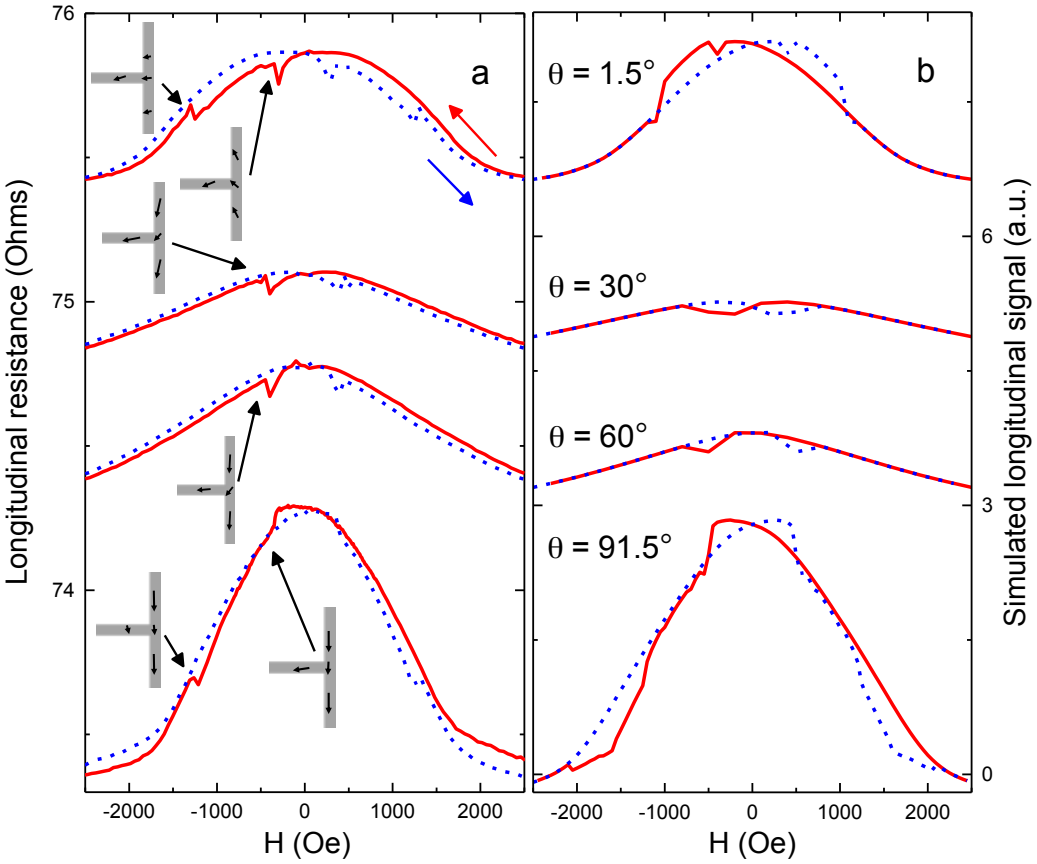


Fig. 8. (a) Longitudinal MR plots of brickwork artificial spin ice at selected angles. (b) Corresponding simulation data for longitudinal MR. From the top, the MR plots are for θ = 1.5°, θ = 30°, θ = 60°, and θ = 91.5°, respectively. Plots except for θ = 91.5° have been shifted upwards for viewing ease. The insets show schematics of the magnetization configurations at different points in the field sweeps.

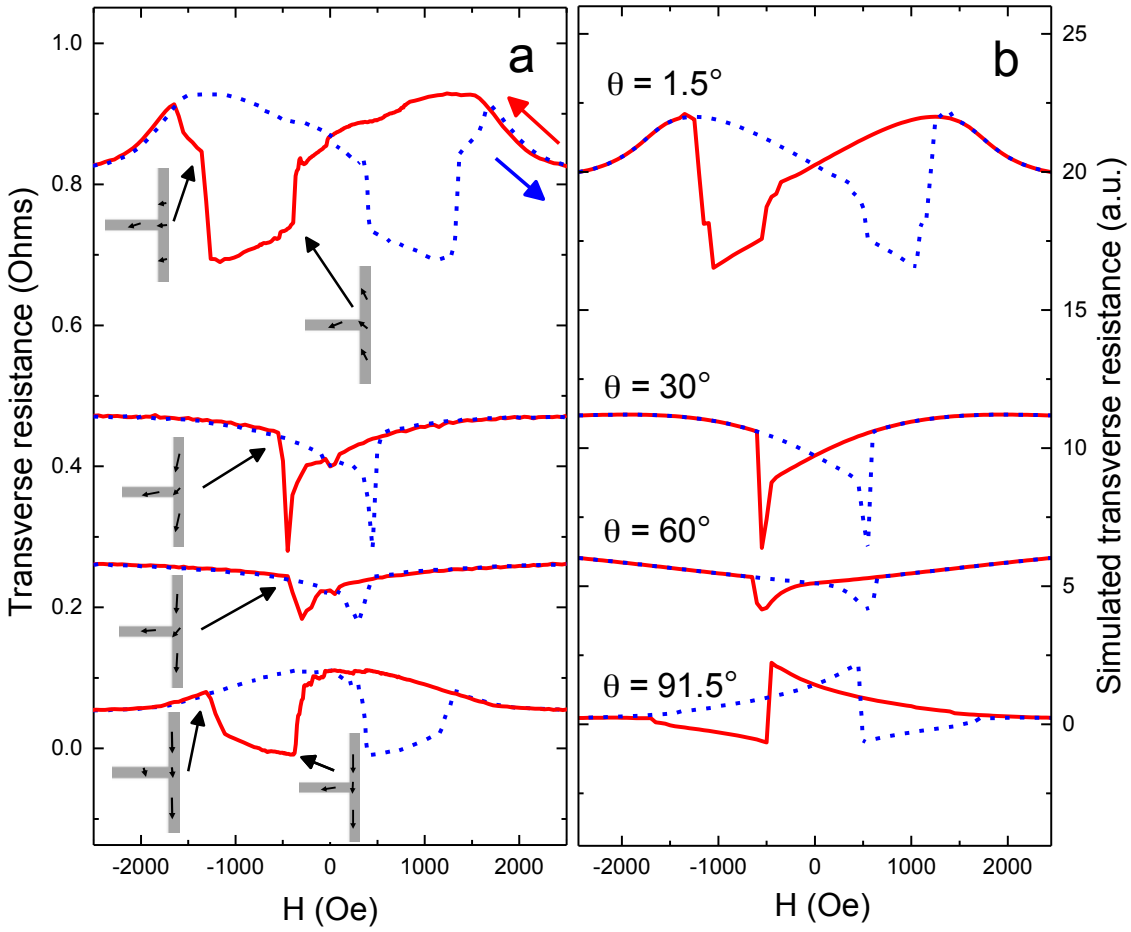


Fig. 9. (a) Transverse MR plots of brickwork artificial spin ice at selected angles. (b) Corresponding simulation data for transverse MR. From the top, the MR plots are for θ = 1.5°, θ = 30°, θ = 60°, and θ = 91.5°, respectively. Plots except for θ = 91.5° have been shifted upwards for viewing ease. The insets show schematics of the magnetization configurations at different points in the field sweeps.

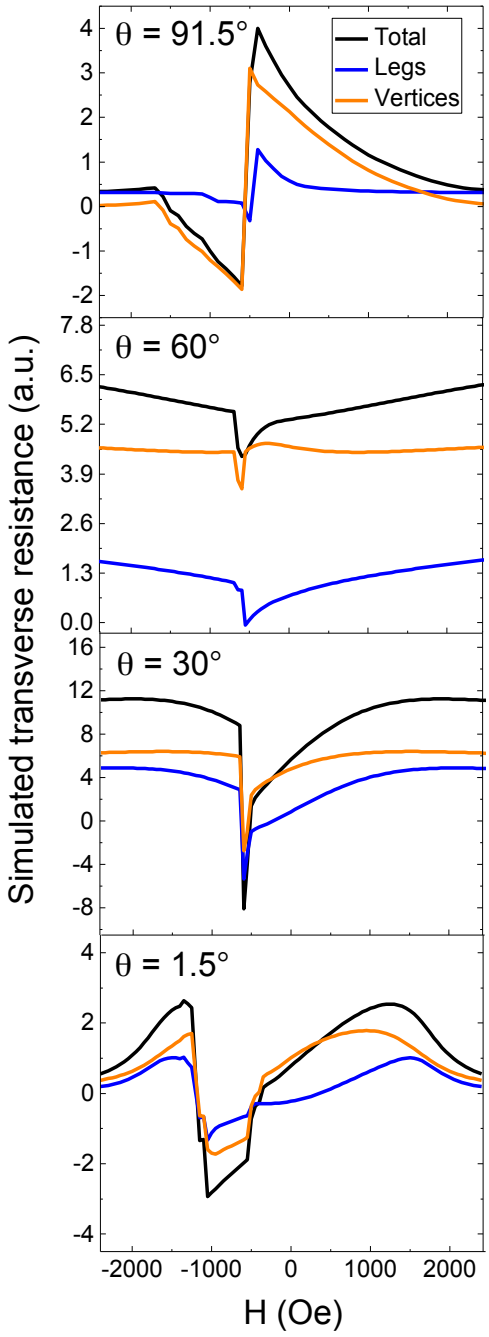


Fig. 10. Nanowire leg and vertex contributions to the simulated transverse resistance, obtained by integrating only over portions of the path. Note the significant contributions from the vertex regions at every angle.

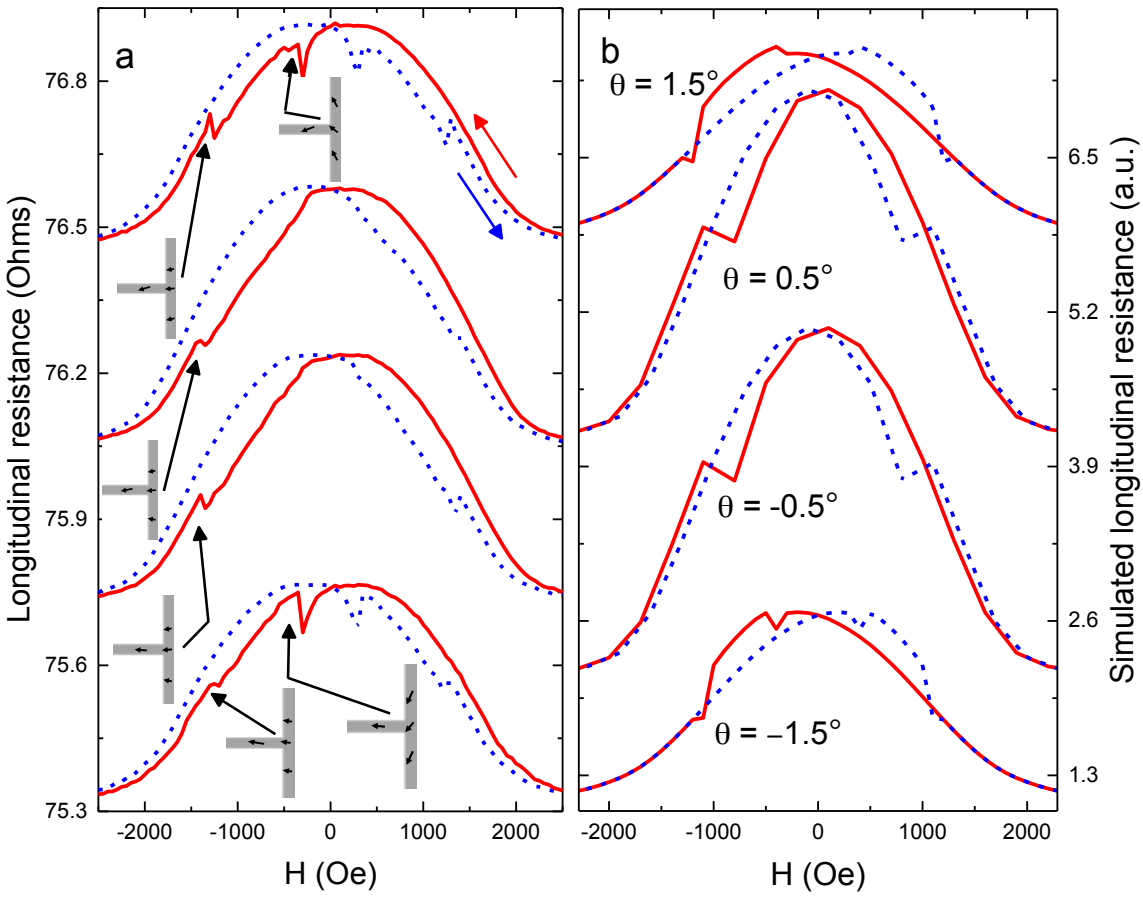


Fig. 11. (a) Longitudinal MR plots at closely spaced angles around θ = 0° (b) Corresponding simulation data for longitudinal MR. Plots except for θ = -1.5° have been shifted upwards for viewing ease. The insets show schematics of the magnetization configurations at different points in the field sweeps.

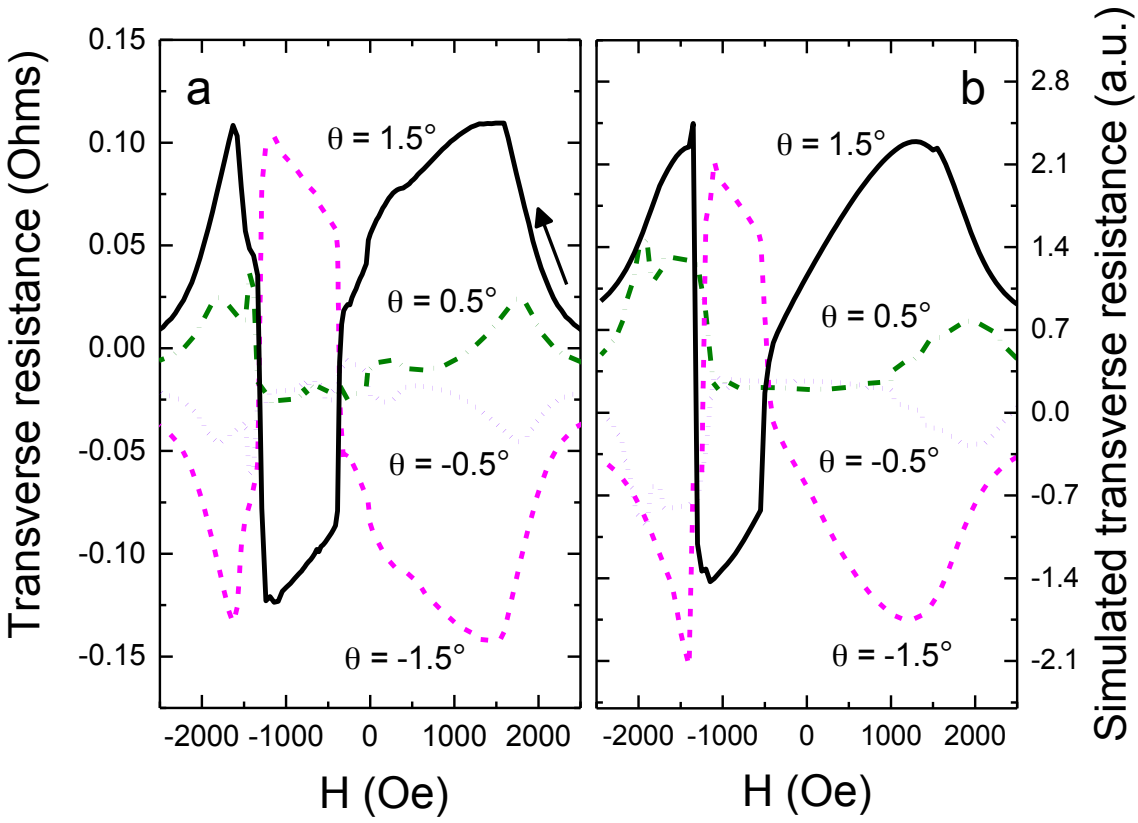


Fig. 12. (a) Experimental and (b) simulated transverse MR during down sweep in small angular steps around θ = 0°. The shape of the plot abruptly changes as the angle approaches closer to 0°. There is also an inversion symmetry between the plots above and below 0°, associated with the reversal of polarization of the moments aligned with θ = 90°.

**Reference**


[1] L. J. Heyderman, and R. L. Stamps, Journal of Physics: Condensed Matter **25**, 363201 (2013).

[2] C. Nisoli, R. Moessner, and P. Schiffer, Rev. Mod. Phys. **85**, 1473 (2013).

[3] I. Gilbert, C. Nisoli, and P. Schiffer Physics Today **69**, 54 (2016).

[4] X. Ke, J. Li, C. Nisoli, Paul E. Lammert, W. McConville, R. F. Wang, V. H. Crespi, and P. Schiffer, Physical Review Letters **101**, 037205 (2008).

[5] R. F. Wang, C. Nisoli, R. S. Freitas, J. Li, W. McConville, B. J. Cooley, M. S. Lund, N. Samarth, C. Leighton, V. H. Crespi, and P. Schiffer, Nature **439**, 303 (2006).

[6] Yi Qi, T. Brintlinger, and J. Cumings, Physical Review B **77**, 094418 (2008).

[7] X. Ke, J. Li, S. Zhang, C. Nisoli, V. H. Crespi, and P. Schiffer, Applied Physics Letters **93**, 252504 (2008).

[8] S. Zhang, J. Li, J. Bartell, X. Ke, C. Nisoli, P. E. Lammert, V. H. Crespi, and P. Schiffer, Physical Review Letters, **107**, 117204 (2011).

[9] J. Li, X. Ke, S. Zhang, D. Garand, C. Nisoli, P. Lammert, V. H. Crespi, and P. Schiffer, Physical Review B, **81**, 092406 (2010).

[10] Y. Perrin, B. Canals, and N. Rougemaille, Nature **540**, 410 (2016).

[11] A. Farhan, P. M. Derlet, A. Kleibert, A. Balan, R. V. Chopdekar, M. Wyss, J. Perron, A. Scholl, F. Nolting, and L. J. Heyderman, Physical Review Letters **111**, 057204 (2013).

[12] S. Zhang, I. Gilbert, C. Nisoli, G. -W. Chern, M. J. Erickson, L. O'Brien, C. Leighton, P. E. Lammert, V. H. Crespi, and P. Schiffer, Nature **500**, 553-557 (2013).

[13] J. Drisko, S. Daunheimer, and J. Cumings, Phys. Rev. B, **91**, 224406 (2015).

[14] V. Kapaklis, U. B. Arnalds, A. Farhan, R. V. Chopdekar, A. Balan, A. Scholl, L. J. Heyderman, and B. Hjörvarsson, Nature Nanotechnology, **9**, 514-519 (2014).

[15] I. Gilbert, Y. Lao, I. Carrasquillo, L. O'Brien, J. D. Watts, M. Manno, C. Leighton, A. Scholl, C. Nisoli, and P. Schiffer, Nature Physics **12**, 162-165 (2016).

[16] I. Gilbert, G. -W.Chern, S. Zhang, L. O'Brien, B. Fore, C. Nisoli, and P. Schiffer, Nature Physics **10**, 670-675 (2014).

[17] L. Anghinolfi, H. Luetkens, J. Perron, M. G. Flokstra, O. Sendetskyi, A. Suter, T. Prokscha, P. M. Derlet, S. L. Lee, and L. J. Heyderman, Nature Communications **6**, 8278 (2015).

[18] Alan Farhan, Andreas Scholl, Charlotte F. Petersen, Luca Anghinolfi, Clemens Wuth, Scott Dhuey, Rajesh V. Chopdekar, Paula Mellado, Mikko J. Alava & Sebastiaan van Dijken, Nature Communications **7**, 12635 (2016).

[19] Y. Li, T. X. Wang, Z.T. Hou, H.Y. Liu, X.F. Dai, and G.D. Liu, Physics Letters A, **380**, 2013-2016 (2016).

[20] B. L. Le, J. Park, J. Sklenar, G. -W. Chern, C. Nisoli, M. Manno, C. Leighton, J. D. Watts, D. W. Rench, N. Samarth, and P. Schiffer, Phys. Rev. B **95**, 060405(R) (2017).

[21] A. S. Wills, R. Ballou, and C. Lacroix, Phys. Rev. B **66**, 144407 (2002).

[22] M. Tanaka, E. Saitoh, H. Miyajima, T. Yamaoka, and Y. Iye, Phys. Rev. B **73**, 052411 (2006).

[23] T. Mcguire, and R. Potter, IEEE Transactions on Magnetics **11**, 1018 (1975).

[24] A. Vansteenkiste, J. Leliaert, M. Dvornik, M. Helsen, F. Garcia-Sanchex, and B. V. Waeyenberge, AIP Advanced **4**, 107133 (2014).

[25] ANSYS® Academic Research, Release 16.0.

[26] W. R. Branford, S. Ladak, D. E. Read, K. Zeissler, and L. F. Cohen, Science **335**, 1597 (2012).

[27] B. L. Le, D. W. Rench, R. Misra, L. O'Brien, C. Leighton, N. Samarth, and P. Schiffer, New J. of Phys. **17**, 023047 (2015).